Chaotic Sensing

Shekhar S. Chandra, *Member, IEEE*, Gary Ruben, Jin Jin, Mingyan Li, Andrew M. Kingston, Imants D. Svalbe, and Stuart Crozier

***Abstract*— We propose a sparse imaging methodology called chaotic sensing (ChaoS) that enables the use of limited yet deterministic linear measurements through fractal sampling. A novel fractal in the discrete Fourier transform is introduced that always results in the artifacts being turbulent in nature. These chaotic artifacts have characteristics that are image independent, facilitating their removal through dampening (via image denoising), and obtaining the maximum likelihood solution. In contrast with existing methods, such as compressed sensing, the fractal sampling is based on digital periodic lines that form the basis of discrete projected views of the image without requiring additional transform domains. This allows the creation of finite iterative reconstruction schemes in recovering an image from its fractal sampling that is also new to discrete tomography. As a result, ChaoS supports linear measurement and optimization strategies, while remaining capable of recovering a theoretically exact representation of the image. We apply the method to the simulated and experimental limited magnetic resonance (MR) imaging data, where restrictions imposed by MR physics typically favor linear measurements for reducing acquisition time.**

***Index Terms*— Fractal sampling, Chaos, sparse image reconstruction, discrete Fourier slice theorem, Ghosts, fractals, missing data, compressed sensing.**

I. Introduction

RECOVERING an image of an object from a set of measurements is of great importance in the physical sciences, engineering and medicine. For example in medicine, medical imaging aids clinicians in diagnosing diseases [1]. This process of image reconstruction, whether from projected views of the object or a transform space such as the Fourier space, is challenging because acquisition is always limited is some sense. The limitations may occur because the imaging modality has high time-cost, such as in magnetic resonance (MR) imaging, or because the instrumentation has a limited range of motion, such as in many biomedical imaging experiments at synchrotron facilities. It could be because the imaging modality exposes the specimen to ionizing radiation and this exposure needs to be minimized, such as in computed tomography (CT). Or it could be because the imaging methods chosen are themselves ill-posed, as with most algorithms utilized in medical imaging [2], [3].

In cases such as these, limited imaging data creates ambiguity about the object and manifests itself as reconstruction artifacts known as Ghosts[1] in the recovered image [3]–[7].

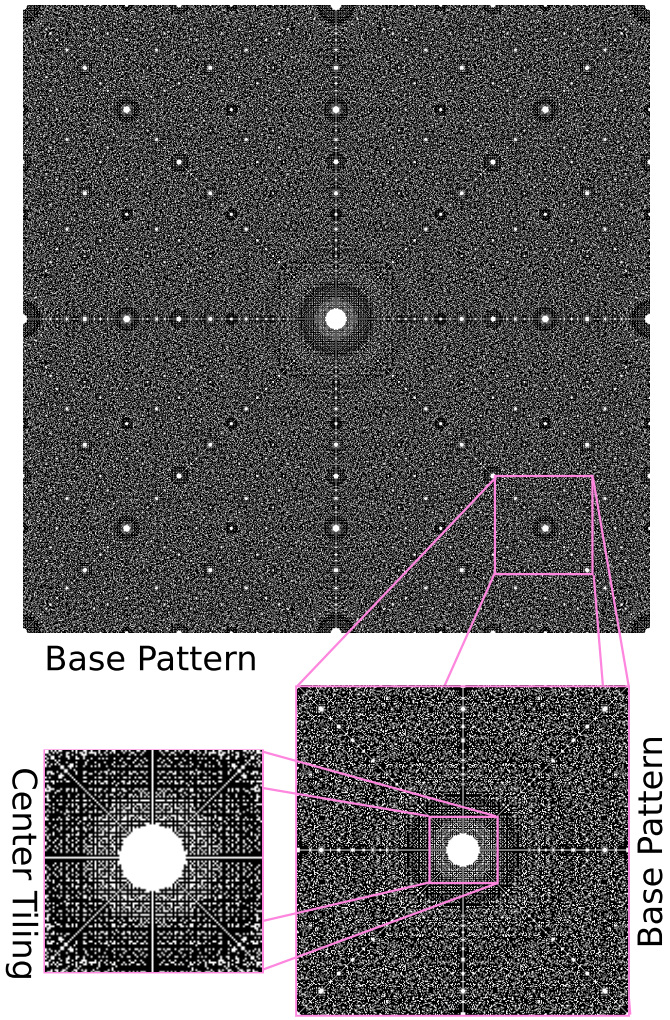

Fig. 1. A schematic of the finite fractal for the DFT introduced in this work. The base pattern is self-similar at multiple scales to create a multi-band response in discrete Fourier space. A high resolution image is available as supplementary material, but details can be seen by zooming in on this figure.

Manuscript received January 15, 2017; revised September 1, 2017, May 3, 2018, and June 21, 2018; accepted July 31, 2018. Date of publication August 10, 2018; date of current version September 17, 2018. The associate editor coordinating the review of this manuscript and approving it for publication was Dr. Denis Kouame. *(Corresponding author: Shekhar S. Chandra.)*

S. S. Chandra, M. Li, and S. Crozier are with the School of IT and Electrical Engineering, The University of Queensland, Brisbane, QLD 4072, Australia (e-mail: shekhar.chandra@uq.edu.au).

G. Ruben and I. D. Svalbe are with the School of Physics, Monash University, Clayton, VIC 3800, Australia.

J. Jin is with the Institute for Neuroimaging and Informatics, University of Southern California, Los Angeles, CA 90007 USA.

A. M. Kingston is with the Department of Applied Mathematics, The Australian National University, Canberra, ACT 2600, Australia.

This paper has supplementary downloadable material available at http://ieeexplore.ieee.org, provided by the author. The material includes supplemental figures. The total size of the file is 1.1 MB. Contact shekhar.chandra@uq.edu.au for further questions about this work.

Color versions of one or more of the figures in this paper are available online at http://ieeexplore.ieee.org.

Digital Object Identifier 10.1109/TIP.2018.2864918

[1] Sometimes referred to as phantoms [4] or ambiguity functions.

These Ghosts have invisible structures in the direction of known measurements and generate visible artifacts corresponding to unmeasured directions [6]. Thus, it is essential that image reconstruction algorithms be able to mitigate these artifacts, preferably with low computational complexity.

In this work, we propose a new approach to sparse imaging called Chaotic Sensing (ChaoS) that utilizes a new fractal for sampling in the discrete Fourier transform (DFT) (see figure 1). The novel contributions can be summarized as follows:

1) The proposed ChaoS method utilizes a deterministic sampling pattern (in the form of a newly proposed fractal) that can be decomposed into discrete tomographic projections while producing artifacts turbulent in nature and therefore appearing independent of the image being recovered. The resulting linear reconstruction methodology handles significantly under-sampled imaging data (shown up to a reduction factor 8), while still recovering the image with promising performance over existing methods.
2) A newly discovered fractal for the DFT is presented (see figure 1) that is formed from discrete linear measurements. This fractal disorders the Ghosts causing them to be turbulent via the frequency domain. The measurements from this fractal also map to discrete projections that forms a periodic sinogram and facilitates efficient reconstruction.
3) Developing novel finite maximum likelihood expectation maximization (fMLEM) and finite simultaneous iterative reconstruction technique (fSIRT) algorithms for complex-valued periodic discrete projections, where the result is obtained via linear optimisation. These finite iterative algorithms also facilitate fast back-projection directly via DFT space because a discrete periodic slice theorem is used that requires no interpolation.
4) We apply the proposed ChaoS methodology to complex-valued MR imaging experimental data of phantoms in the form of simulated fractal sampling of the data and compare the results to other sparse imagingc methods.

A fractal is a self-similar pattern or structure that repeats itself on multiple scales. They have an associated "roughness" that classifies them with a fractional or Hausdorff dimension and was first formally introduced by Mandelbrot [8] (see also [9]). They are a subset of a large body of work called chaos theory or complex dynamical systems developed independently by Lorenz [10], Feigenbaum [11] and others, who found that deterministic systems exhibit non-periodic, high entropic behavior with a sensitive dependence on initial conditions.

We employ the term "turbulent" in a technical sense to represent the chaotic mixing of imaging information that is self-similar at multiple scales, i.e. the image is convolved with a fractal point spread function (PSF). This is analogous to the dissipation of energy at large scales and low frequencies into many smaller scales and higher frequencies within fluid flow that can lead to chaotic motion [12] and conform to stable solution spaces that have to be fractals [10], [12]. Our intuitive usage of the term is best summarized by Richardson [13] in a famous comment on atmospheric turbulence.[2]

The goal is to make self-similar, multi-scale yet deterministic measurements that promote disordered artifacts in the recovered image using fractals. Since the object is consistent within the measurements, the disorder is removed through (linear) reconstruction schemes. Advantages of the proposed scheme include:

1) more practical realizations in the laboratory. For example within MR imaging, by exploiting the underlying geometry of the measurements via fractals, such as a set of discrete periodic lines in our case,
2) sparse methods that support faster, linear image reconstruction by way of projections of the object,
3) no need for additional sparse transform domains,
4) governed by an exact uncertainty principle [6], [14], so that the reconstructions are guaranteed to be void of Ghost artifacts that are mentioned by Herman and Davidi [15] when the prescribed imaging information is utilized,
5) fast iterative reconstruction with low computational complexity through using a discrete periodic slice theorem.

After presenting the current literature in image reconstruction with missing or limited data, the proposed methods are presented in section II with the results of MR imaging focused simulations and experiments thereafter and a discussion of these findings in section IV.

A. Previous Work

Traditional methods for handling Ghost artifacts involve using either a large number of measurements to compensate [5], iterative schemes based on algebraic reconstruction [16], [17] or expectation maximization (EM) algorithms [18]. This is especially true when signal-to-noise ratio (SNR) and photon counts are low such as in positron emission tomography (PET) [19]. Popular algorithms in these scenarios include the EM algorithms [19] and their extensions for accelerated convergence [20], better image quality [21] and arbitrary image pixel depths [22]. Image reconstruction methods can even be created that learn their characteristics to remove them given enough training data [23]. Other methods for reducing Ghosts include fusion of multi-modal data [24], minimizing the ℓ_1-norm in reconstructions [25], [26], solving certain system of equations [27] or by fast direct deconvolution of Ghost artifacts if no noise is present [28]. See Chandra *et al.* [28] for a summary of the work in Ghosts during the last century.

The most significant progress towards reducing and even eliminating Ghost artifacts was made independently by Candès *et al.* [29] and Donoho [30], an area now known as compressed sensing (CS). In their approach, the acquired data is structured or acquired with random sampling so that the

[2] "Big whirls have little whirls that feed on their velocity, and little whirls have lesser whirls and so on to viscosity" - Richardson, 1922 [13].

Ghosts are incoherent in the reconstructed space and convex optimization is used to effectively minimize or threshold out their effects [31], [32]. Combined with transform sparsity, i.e. a transform space where the number of bases needed to represent the object is very small with respect to the total number of bases in the space, the signal can be acquired and recovered with fewer samples than the Nyquist sample rate [30]. This measurement is then a compressed form of the signal without significant loss of data. The signal is usually recovered using methods such as iterative thresholding [33], basis pursuit [34] or orthogonal matching pursuit [35]. This approach has been successfully applied to MR imaging [36], [37] and other areas of imaging [38], [39]. See Eldar and Kutyniok [32] for a detailed review of CS.

However, CS has four important considerations:

1) random sampling is not always practical in some systems. In MR imaging for example, three and two dimensional (2D) random sampling of k-space is not practical because of the MR hardware and sequence protocol limitations. Since random sampling in the frequency-encoding direction is impractical, the incoherence due to one dimensional (1D) random sampling is reduced, leading to reduced undersampling ability and reconstruction fidelity.
2) transform sparsity is required, but ideally not in measurement space. In MR imaging for example, anatomical objects are usually not suitably sparse in k-space [40], [41], requiring dense sampling near the central k-space region. Therefore, the measurement data is transformed into a transform space where the image is sparse and the artifacts remain noise-like, such as the wavelet domain.
3) non-linear reconstruction algorithms such as convex optimization or basis pursuit algorithms have high computational complexity relative to the fast Fourier transform (FFT) [42] and still are a subject of active research [37], [43].
4) Herman and Davidi [15] showed that Ghost artifacts may remain hidden with respect to the projected views, although clearly visible within the image as a strong artifact (see [15, Fig. 2]), when a small number of projections are used. These artifacts could have important implications in a medical setting.

The proposed ChaoS provides a methodology that does not require a transform domain or even assume the image is highly compressible under certain conditions. It can utilize limited linear measurements in DFT space and still produce image independent artifacts. These artifacts can be removed using computationally efficient reconstruction algorithms, and results in a theoretically exact image of the object under prescribed conditions.

II. Chaotic Sensing

The fundamental principle behind the proposed ChaoS methodology is to promote deterministic disorder in the reconstructed image and chaotic mixing of imaging information created from limited measurements. Since the image is assumed consistent within the measurements, any resulting artifacts from the reconstruction process will be turbulent. We utilize the image independent nature of these artifacts to allow the dampening and eventual removal of these artifacts. An important application area of the proposed methodology is MR imaging, which is time-expensive because it is currently a slow imaging modality and scanners cost millions of dollars. To reduce the MR acquisition times, sparse imaging methods that preserve image quality are sought.

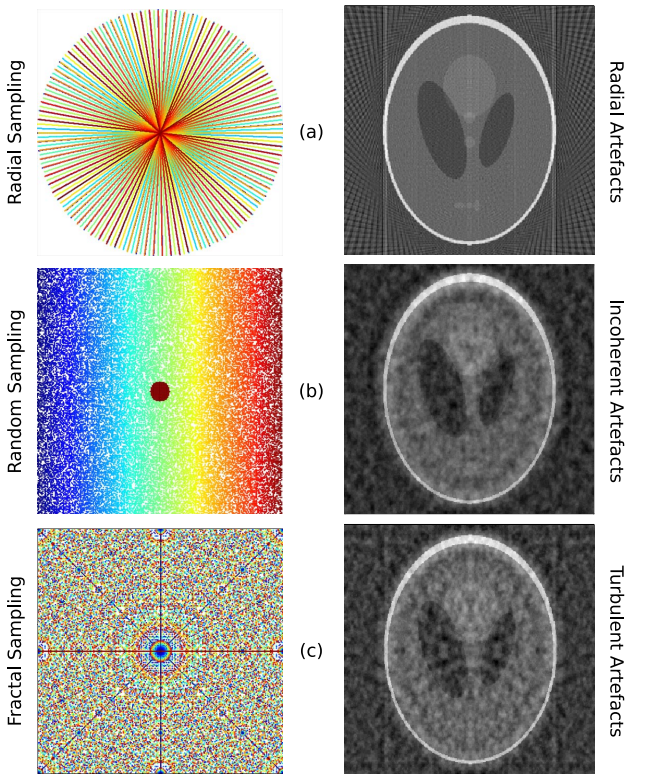

Fig. 2. The Ghost artifacts as a consequence of various sampling methods in DFT space. From top to bottom, the artifacts due to a radial sampling, random sampling and the proposed fractal sampling before any algorithms are applied. Each color in the sampling plots on the left represent the same sample line. These lines are radial lines, columns and discrete slices for (a), (b) and (c) respectively. The proposed method naturally produces artifacts with little discernible structure while using discrete periodic lines in DFT space.

A. Discrete Fourier Ghosts

The excellent soft tissue contrast in MR imaging is obtained by measuring the radio frequency (RF) electro-magnetic waves produced by Hydrogen atoms through spatial density (spatially varying, nuclear spin harmonic), response to external magnetic fields and the relaxation properties. The RF measurements results in a harmonic representation equivalent to that of the DFT of the object that is also referred to as k-space in the literature. The difficulty is determining the most time efficient coverage or tiling method of 2D DFT space to facilitate a suitable recovery of an image of the object.

However, when only a partial coverage of the DFT is available, artifacts become superimposed on the recovered image [4]. The shape and form of these Ghost artifacts are dependent on the structure(s) of the missing coefficients in

DFT space, since errors in DFT space are convolved in image space because of the convolution theorem [3]. Figure 2 shows a comparison of the Ghosts produced by the proposed method compared to two common strategies in MR imaging.

The imaging methods based on CS rely on the measurements being made in a particular sampling pattern to ensure that the artifacts superimposed on the recovered image are incoherent, i.e. the artifacts have a random or white noise-like structure [30]. A random sampling pattern is usually employed to ensure that the artifacts are also random in nature (see figure 2(b)). The image is then recovered by effectively compressing the reconstruction and denoising the result iteratively. The compression is obtained by assuming the image is known to be sparse or in another transform domain. Wavelets have been shown to work well with MR imaging data [36].

However, true random sampling in MR imaging is impractical (see [44, Sec. 2.1.4]). To resolve the spatial origins of the spins, spatial encoding signals are embedded into the decay signals. To this end, frequency encoding (small frequency offset δ_f) is introduced into one of the dimensions by superimposing a magnetic field gradient along this dimension during the measurement. To resolve additional dimension(s), phase encoding (δ_p) by means of spatially dependent phase offset is used. It is typically achieved by introducing frequency offsets δ_f of determined duration T ($\delta_p = \delta_f \cdot T$) immediately before the measurement. Typically, repeated measurements with identical timing albeit varied phase offsets are performed to resolve the 2nd or 3rd dimension. Since the decay must complete and steady state be reached between measurements, a measurement cycle incurs a fixed time cost. This means that measurements made (phase-encoding direction) where another decay is required are time expensive, while those made within a decay period (frequency-encoding) are cheap. Therefore, CS based methods rely on incoherence in usually only one dimension, by acquiring full phase encoding directions randomly and a transform domain for 2D incoherence being still applicable [36]. This results in a lower fidelity reconstruction when compared with 2D incoherence as with a full CS solution [44]. As a result, despite being more than a decade since its inception, there are only a few CS based MR methods commercially available as MR imaging clinical sequences.

B. Turbulent Ghosts

The proposed ChaoS provides a methodology that does not require a transform domain. It can utilize limited linear measurements in DFT space and still produce object independent artifacts. These properties are made possible because of fractal sampling.

1) Fractals: Fractals are constructed from a set of simple deterministic rules, yet exhibit complex behavior at multiple scales. For example, the Sierpinski carpet is formed by simply dividing a rectangle into 9 equal parts and removing the center. The process is repeated with the remaining rectangles *ad infinitum* to produce a pattern that has an area of zero. This particular fractal sees repeated use in RF design [45] and more recently in MR imaging hardware [46]. Other examples include the Cantor set, the Terdragon set, the Mandelbrot set and the Julia sets. An example of a Julia set [47] is given in figure 3. In this work, we will create a new fractal for the DFT shown in figure 1 and described in the next section.

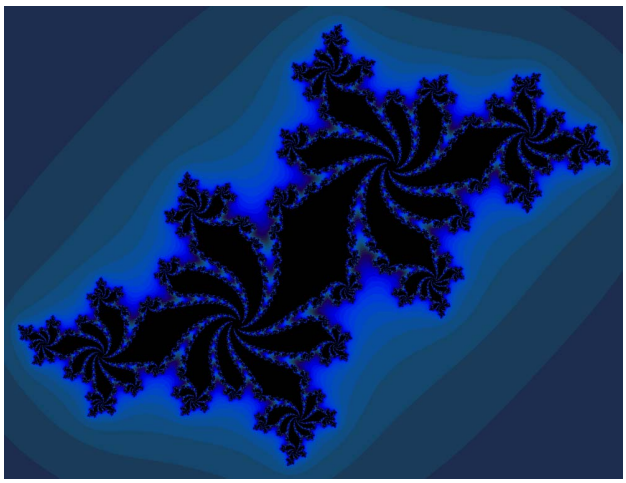

Fig. 3. An example of a fractal known as the Julia set [47] for a given constant/offset c. Available in color in the online version of this article.

2) Fractal Frequency Response: Examining the fractal in figure 1, the base pattern of this fractal in discrete Fourier space repeats itself at multiple scales with finer and finer resolutions at higher Fourier frequencies. This produces a multi-band response in image space, in the same way as fractal antennas were designed [45]. These antennas are capable of receiving and transmitting at multiple bands because they have the same shape, i.e. it is self-similar, at the required (different) scales for those frequency bands.

3) Turbulence: In image space (after an inverse DFT is applied to the measurements) the image is effectively convolved with a fractal PSF causing turbulence and ensuring mixing of artifacts.This turbulence is the same phenomenon that is responsible for allowing golf balls to travel greater distances when struck. The dimples of the ball disrupts airflow, dissipating the energy of the oncoming air. Otherwise, the laminar flow into the ball would create high pressure and push against the low pressure behind the ball to slow its progress. Likewise, the chaotic mixing of an image or fluid with self-similarity at multiple scales, i.e. it exhibits flow of energy from large scales to smaller scales, then from smaller scales to even smaller ones and so on. It can be viewed as the dissipation of energy with a power spectrum that follows a Kolmogorov power-law with length scale or equivalent to how eddies form in fluid flow and how energy is dissipated at higher and higher wave numbers. Therefore, the fractal ensures artifacts do not correlate or cascade into meaningful structures, particularly those that are image dependent. Figure 4 shows how the incoherent and turbulent artifacts from figure 2(c) have similar visual characteristics. We will measure the turbulence using a metric called turbulent intensity τ, which is the standard deviation of the velocity fluctuation $\vec{v} = g - \bar{g}$, where $g = \nabla I$ is the image gradient and $\bar{g}$ is the mean of g.

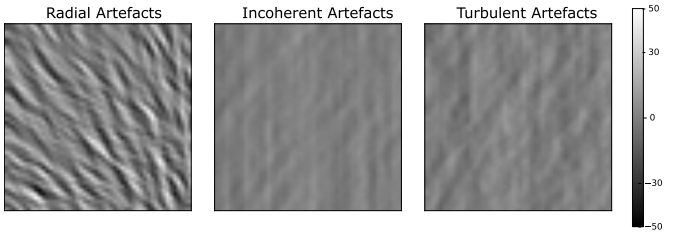

Fig. 4. The velocity fluctuations of the artifact gradient vector fields from the radial, random and fractal sampling schemes of the top left-hand corner of the images in figure 2.

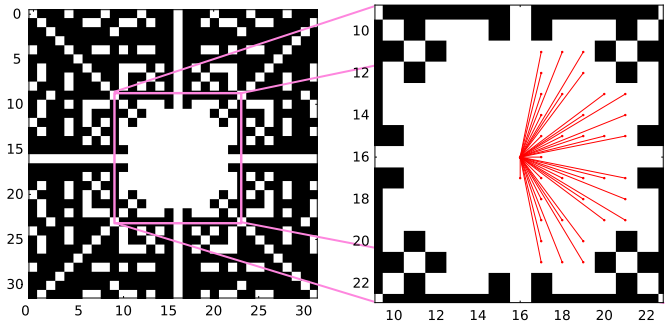

Fig. 5. The tiling effect of the ℓ_2 minimal Farey sequence (i.e. sorted vectors from (1)) visualized in the image plane as a binary image using the discrete lines (2) for $\mathcal{N} = 8$ and $M = 32$. The inset shows the closest vectors $[b, a]$ visible from the (centerd) origin used to generate the lines.

It is also well known that turbulent flows conform to "attractors" in phase space, a space defined by the main parameters of the equations of motion describing the system, and these attractors have to be fractals in the case of turbulence [10], [12]. An attractor is a shape or structure in phase space that the system evolves to when in steady state. One of the famous attractors is known as the Lorenz attractor from a study of atmospheric sciences, where the system follows an owl head like structure never traversing the same path on that structure but always attracted to that structure no matter the initial conditions [10]. The fractal in the DFT creates turbulence to ensure a mixing of artifacts that give it a disorderly appearance in much the same way that Ruelle and Takens [12] found that turbulent motion is a mathematical consequence of fractal structures when analyzing the equations of motion of fluids. In this work, we take the reciprocal view that a fractal in frequency space, i.e. in the DFT, will create a chaotic mixing of imaging information by the way of circular convolution of the image with the fractal structure.

C. Finite Fractal

The chaotic mixing of image information is dependent on the fractal structure in DFT space. In this work, we will create a new fractal for the DFT shown in figure 1. Note that the Python implementation of the proposed methods and associated algorithms are provided as an open source project [48].

To construct this new finite fractal for the DFT, recall that the majority of the power of DFT space of natural images lies near the origin (i.e. the DC coefficient). Therefore, to ensure that we can adequately represent and reconstruct natural images, we require a set of closest lattice points (b, a) visible from the origin to tile the central DFT region. These lattice points (b, a) can be defined as the set of irreducible rational fractions a/b of the Farey sequence, where $a, b \in \mathbb{Z}$ and $\gcd(a, b) = 1$ (i.e. a and b have no common factor other than unity) [49]. We can interpret a Farey fraction as a vector $[b, a]$ (i.e. a pixels across and b pixels up) in DFT space.

To generate this set of tiling lattice points near the origin (in one octant of the plane) of order $\mathcal{N}$, we simply use the mediant property of the Farey sequence [49] to generate all the irreducible vectors and then sort these vectors by their $\ell_2 = a^2 + b^2$ norm, i.e. the Euclidean distance from the origin, to select the closest ones. This set of vectors and their multiples then tile a circular region around the origin. These vectors correspond directly to the $\mathcal{F}_\mathcal{N}$ Farey sequence of fractions. Beginning with $[b_1, a_1] = [1, 0]$ and $[b_2, a_2] = [1, 1]$, to obtain the mediant lattice point $[b_3, a_3]$, one recursively computes

$$\frac{a_3}{b_3} = \left(\frac{a_1 + a_2}{b_1 + b_2}\right), \tag{1}$$

until $[b_3, a_3] = [\mathcal{N}, 1]$ and any other (soon to be mentioned) criteria is met. Direct computation can be done using well-known methods such as Pascal's Triangle (with memory) or by equations that solve for the subsequent term. Symmetry of the Farey sequence in an octant of the plane is used to create the vectors for all other octants using simple flip and mirror operations. For example, when $\mathcal{N} = 3$, the generated set (in the half plane) is

$$\begin{aligned}
&[1, 0], \quad [1, 1], \quad [-1, 1], \quad [2, 1],\\
&[1, 2], \quad [-2, 1], \quad [-1, 2], \quad [3, 1],\\
&[1, 3], \quad [-3, 1], \quad [-1, 3], \quad [3, 2],\\
&[2, 3], \quad [-3, 2], \quad [-2, 3], \quad [0, 1].
\end{aligned}$$

The extent of the tiling near the origin is controlled by $\mathcal{N}$, which tiles a small aperture near the origin (see inset of figure 5). In fact, the tiling of the origin and its relation to reconstruction properties are controlled by a criterion that will be defined in the next section. We can then associate the set of discrete lines with slopes defined by these fractions as

$$\Gamma_{t,\theta_{ab}} = \begin{cases} t = bv - au & \text{if } \dfrac{a}{b} \geqslant 0 \\ t = au - bv & \text{if } \dfrac{a}{b} < 0, \end{cases} \tag{2}$$

where the line is at an angle $\theta_{ab} = \tan^{-1}(a/b)$. The lines (2) are radial if we set $t = 0$ and ensure that all points multiple to the irreducible vectors of the Farey sequence are covered. An example of the generated vectors for $N = 8$ within a larger image $M = 32$ and an example of their resulting lines are shown in figure 5.

Finally, to form the fractal shown in figure 1, we simply compute the modulo N of the point coordinates for the lines, i.e. $(\mathrm{mod}\, N)$, to ensure any points outside the image wraps back into image space. The $(\mathrm{mod}\, N)$ operator is a form of clock arithmetic that leaves only the remainder. For example,

the time 1 pm is a result of 13 modulus 12. This operator is responsible for creating circular boundary conditions so that lines always remain within a fixed image space. Due to these boundary conditions, only a total of N points per line are required as they repeat after a period of N by design. An example of the fractal created by algorithm 1 for $N = 4127$ and 284 discrete lines is provided as supplementary material.

Although the lines (2) are used to create the fractal of figure 1, we can map the slopes of these lines to a more convenient set of periodic lines to facilitate simpler reconstruction using a discrete Fourier slice theorem [50]. In this work, we will assume that for which $N = p$, where p is prime to simplify the reconstruction process.

D. Finite Iterative Reconstruction

The primary objective of the proposed reconstruction methods is to de-construct the measurements of the finite fractal into discrete periodic lines from which it is constructed to the natural discrete slices of the DFT [50], [51]. The discrete Fourier slice theorem (dFST) is a mechanism by which the 2D DFT can be tiled completely and exactly without the need for any interpolation using discrete periodic lines or slices

$$v \equiv mu + t \pmod N, \tag{3}$$

$$u \equiv psv + t \pmod N, \tag{4}$$

with the set of slopes

$$\boldsymbol{m} = \{m : 0 \leqslant m < N,\ m \in \mathbb{N}\}, \tag{5}$$

$$\boldsymbol{s} = \{s : s < {}^{N}/_{p},\ s \in \mathbb{N}\}, \tag{6}$$

of a $N \times N$ image and where $u, v, m, s, t \in \mathbb{Z}$. It has the simplest form above when $N = p$, where p is prime, so that $s = 0$ and the number of slices required to tile the entire space is $N + 1$. An example of the prime size $N = p = 5$ tiling is shown in figure 6. It has been shown previously that the Farey sequence is intimately linked to the slopes $\boldsymbol{m}$ of the DFT slices and that there is a many-to-one mapping between them [52]. Chandra *et al.* [53] developed an exact analytic mapping from a Farey vector to the slope m as

$$m \equiv ab^{-1} \pmod N, \tag{7}$$

where b^{-1} is the multiplicative inverse of b so that $1 \equiv bb^{-1} \pmod N$, which can be computed easily via the extended Euclidean algorithm [49].

Much the same way as the conventional slice theorem of the Fourier transform (FT) in integral form, the inverse DFT of the slices are (periodic) projections of a discretised Radon transform called the finite Radon transform or discrete Radon transform (DRT) [50]. The slices of the DFT $F(u, v)$ are then transformed exactly into a discrete periodic projection space $R(m, t)$ that forms a periodic sinogram. The slices and the projections of the DRT are effectively duals of each other utilizing the same lines (3) and (4) with only a 1D DFT of sequences and a 90 degree rotation of the coordinate system between them [50].

The periodic sinogram $R(m, t)$ of the DRT is obtained by extracting the slices of the DFT and computing the inverse

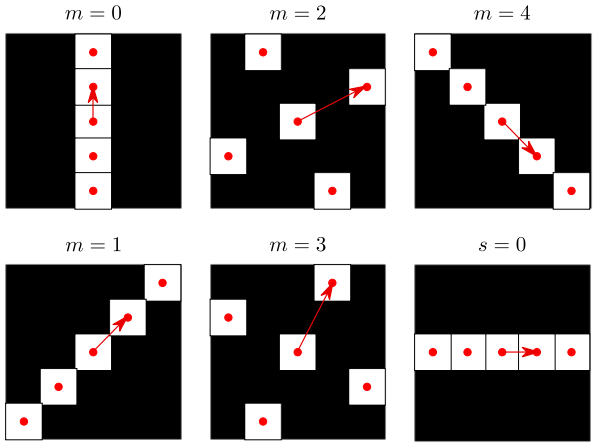

Fig. 6. The tiling of discrete lines defined by equations (3) and (4) for a prime-sized DFT space of $N = 5$ with $t = 0$. Here the DC point is centerd and each white square (and red dot) represents a sample. The lines have slopes according to the set $\boldsymbol{m} \pmod N$ with the slope being m steps up and one step across. The equivalent Farey vectors, i.e. shortest distance from the DC, are shown as red arrows.

1D DFT of each slice. Since the slices of the DFT, and therefore $R(m, t)$ space, does not require any interpolation, the back-projection requires no interpolation either and so it can be computed as a convolution without any interpolation error. This is referred to as circulant back-projection (CBP), since the result is a superposition of circulant matrices [54]. Adding slices to the DFT is $O(\mu N)$, where μ is the total number of measured slices and there are at most $N + 1$ slices. Computing the 1D FFT, which has the order of $O(N \log N)$, the total computational complexity of back-projection of the periodic sinogram is $O(N^2) + O(N^2 \log N)$, since μ is at most order N. Taking the highest order, the total complexity of the algorithm is $O(N^2 \log N)$ for a $N \times N$ image, which is same as the 2D FFT. Therefore, it is possible to create fast reconstruction schemes to the periodic sinogram by constructing finite projection and back-projection operators in DFT space.

We propose novel fast fMLEM and fSIRT algorithms for periodic projections that can be intuitively seen as the iterative back-projection correction on the periodic sinogram via the EM and algebraic algorithms, the former of which is guaranteed convergence to the local maximum of the likelihood function and hence the global maximum when the function is convex [18]. In most practical applications, the EM algorithm is known to always converge to the global solution [55].

Following a similar notation to Lalush and Wernick [56], but adapted to periodic projection and back-projection, let the measured (partial) periodic sinogram from the fractal be represented as g_j, the DRT projection as the operator $\boldsymbol{R}$ and the DRT back-projection as the operator $\boldsymbol{R}^{-1}$, then the fMLEM estimate of the image f at iteration $n + 1$ can be written as

$$f^{n+1} = \frac{f^n}{\mu} \cdot \boldsymbol{R}^{-1}\left(\frac{g_j}{\boldsymbol{R} f^n}\right). \tag{8}$$

Likewise, the Landweber-type fSIRT estimate of the image can be obtained in a similar way. Figure 7 shows a flowchart representation of the reconstruction algorithm.

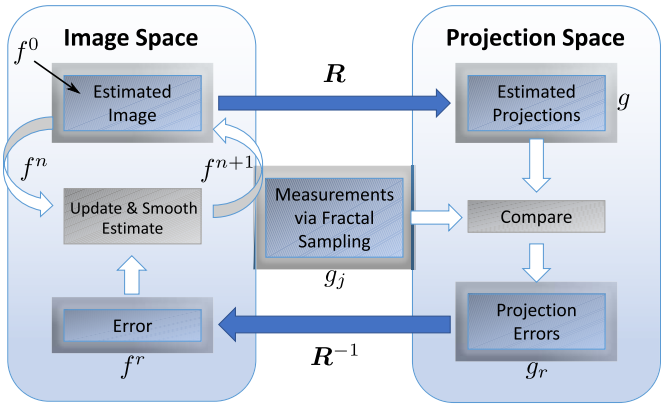

Fig. 7. The (linear) fractal image reconstruction algorithm used in this work, where $g = \boldsymbol{R} f^n$, $f^r = \boldsymbol{R}^{-1} \cdot g_r$ and $\boldsymbol{R}$ is the DRT (i.e. periodic projection) operator.

In these methods, the Ghosts due to under-sampling are removed through a combination of obtaining the most likely solution to the imaging data acquired and dampening of the Ghosts through (edge preserving and/or textural) smoothing. This is made possible because the Ghosts are turbulent and image independent in nature, so that consistent parts of the image is preserved and the method converges to a solution close to the original image. In our implementation, we taper the smoothing off at two stages (mid and end) as the final solution is obtained. Python implementations of the reconstruction algorithms are provided open-source [48].

Note that the normalization terms in (8) are simple scalars, in contrast with conventional iterative methods, where it is an image of back-projected ones at the same angles as the sinogram. In a classical scenario, the back-projection operator is continuous and windowed, so that the image is not uniformly sampled. In the finite case, the circulant matrices cover the entire space evenly because the lines (3) form the basis of periodic projections for the set of all translates

$$\boldsymbol{t} = \{t : t < N,\ t \in \mathbb{N}\}. \tag{9}$$

Hence the weightings become a scalar proportional to the number of projections μ.

Another contribution of our work on the fMLEM and fSIRT is that the projection and back-projection operators $\boldsymbol{R}$ and $\boldsymbol{R}^{-1}$ are fast, since they can be computed in DFT space without the need for interpolation [50]. Projection $\boldsymbol{R}$ is simply computed by taking the 2D DFT of the image, extracting the discrete slices and computing their 1D inverse DFTs. Similarly, back-projection $\boldsymbol{R}^{-1}$ is computed by placing the 1D DFTs of the projections into an empty 2D DFT space and computing the 2D inverse DFT. Thus, the total computational complexity of the proposed method is $O(IN^2 \log N)$, where I is the total number of iterations required for convergence. Utilizing the convergence acceleration of the ordered subsets [20] to both algorithms usually results in $I \leqslant N$.

Lastly, one needs to consider the uncertainty principle for the number of slices required for accurate reconstruction.

Algorithm 1 Fractal Measurements for Finite Iterative Reconstruction

1: $M \leftarrow kN$ for $N \times N$ DFT space. ▷ k controls sparseness/fidelity
2: $p \leftarrow$ nearest prime greater than M.
3: $K \leftarrow 1$ or greater ▷ K controls redundancy/tiling
4: Generate Farey ℓ_2 sequence of order N and K ▷ Use (1)
5: Map each $[b, a]$ to their corresponding m-values. ▷ Use (7)
6: Add finite line for each m-value to space ▷ Use (3)
7: **return** sample or coordinate points belonging to fractal set

The number required is dictated by the Katz criterion

$$K = \frac{\max\left(\sum_{j=0}^{\mathcal{N}-1} |a_j|, \sum_{j=0}^{\mathcal{N}-1} |b_j|\right)}{N}, \tag{10}$$

where usually $K \geqslant 1$. The minimal information required for an exact reconstruction is known to be when $K = 1$ [6], [14]. This intuitively means that the number of bins, or equivalently the number of equations, is equal to the number of pixels that need to be reconstructed. This can be used as an additional termination criteria for generating the Farey sequence and the fractal. Thus, the full algorithm to compute the measurements using the finite fractal of the DFT follows the simple and deterministic rules as given in algorithm 1. A fractal of a size greater than that original image being measured with $k > 1$ allows for exact reconstruction (i.e. when aiming for fidelity and not sparseness), so that the entire space is not tiled by the slices of the DFT. In this work, we have found that the prime p nearest to, but larger than $2N$ usually suffices for this purpose. We demonstrate the proposed ChaoS methodology in the following section.

III. Results

To demonstrate the performance and properties of the proposed ChaoS method, the turbulent nature of the Ghosts were studied, the finite fractal was analyzed and MR simulations of the proposed ChaoS method conducted for reconstruction images from limited Fourier coverage. Lastly, an MR experiment was conducted on a phantom scanned using a Bruker BioSpec 94/30 small animal 9.4T MR scanner (Ettlingen, Germany).

A. Turbulent Ghosts

Firstly, the disorderly or turbulent nature of the Ghosts created using the finite fractal (i.e. sampling that still utilizes discrete radial lines and center tiling) were compared to the conventional radial type sampling and the random sampling of CS that produce incoherent Ghosts. The total number of samples was kept constant for all three types of sampling and the Ghost artifacts observed without any attempt to remove them. Figure 2 shows a comparison of the Ghosts produced by the proposed method compared to these strategies for the Shepp-Logan image.

The turbulent intensity τ of different Ghosts, such as those of figure 2, were compared for a number of images. Figure 4 shows how the incoherent and turbulent artifacts from figure 2(c) have similar visual characteristics. The incoherent and turbulent artifacts were found to have a similar τ, while

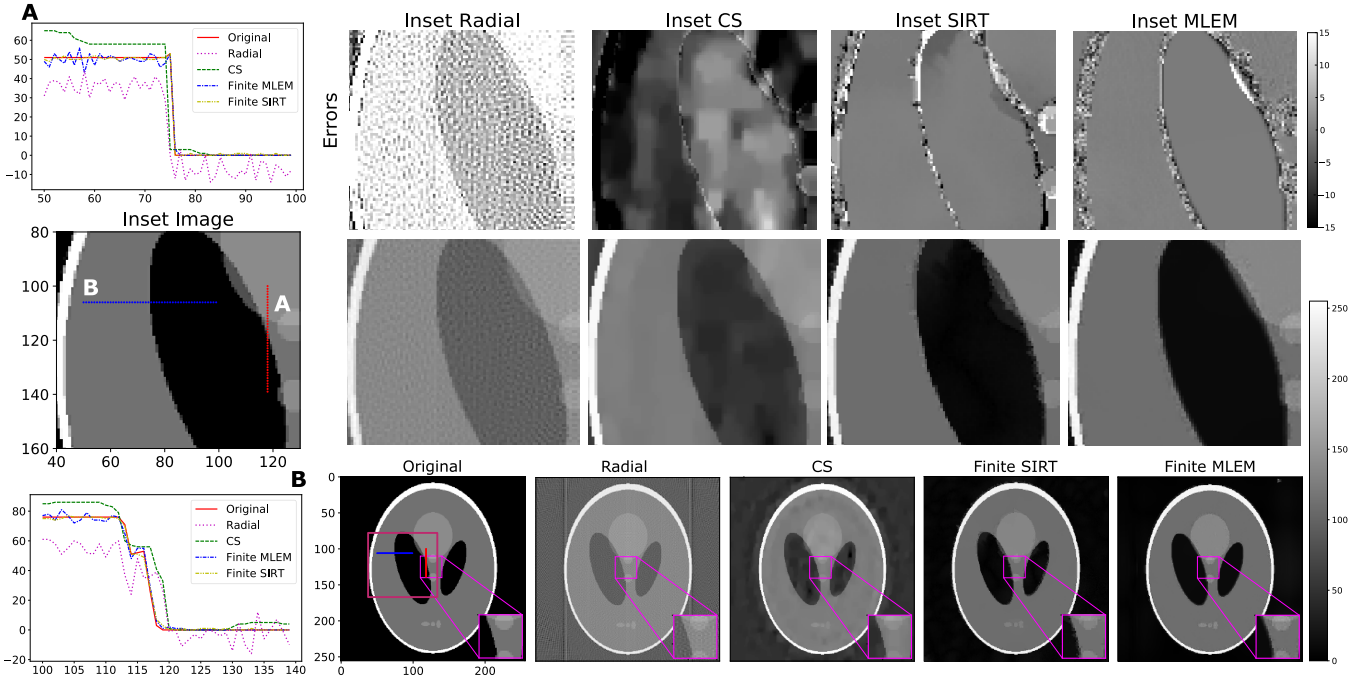

Fig. 8. Reconstruction performance of the proposed, radial and CS methods for recovering the Shepp-Logan phantom from its simulated MR measurements. The synthesized k-space with Gaussian noise had a SNR of 30dB and sampling patterns with a reduction factor of 2 (i.e. 50% of full DFT sampling) were used. The sampling patterns and initial Ghosts are given in figure 2 and the images were gamma corrected for visualization with $\gamma = 0.5$. The image sizes of $N = 256$ and $p = 257$ were used for the CS and finite iterative methods respectively with the latter using a fractal with 128 discrete periodic lines.

both always being a few orders of magnitude different to the radial artifacts. This property of the turbulent Ghosts was also observed for the Cameraman and Lena images.

B. Finite Fractal

The fractal created in this work for $p = 257$ was found to have a fractal dimension of 1.79 using the box count algorithm. The dimension being closer to two rather than to the dimension of its constituents, i.e. the discrete lines, points to the fact that the fractal transcends considerations of just discrete lines and must be thought of as a collective entity. For example, the spacing between the individual points of each periodic line may be very large and their individual effects could be considered with respect to the Ghosts, but their collective effect in tiling at multiple scales with other lines to create the fractal supersedes these effects to produce turbulence.

The fractal also had the remarkable property that it is invariant under DFT and inverse DFT transforms, i.e. it is the same in discrete Fourier and image spaces. The invariance of the finite fractal to the DFT is probably due to the strong symmetry of the geometry structure, which is not only in rotational symmetry, but in modular/periodic symmetry as well, as all periodic lines begin and end as the same point due to the finite geometry of DFT space. Very few functions have such strong symmetry to remain unchanged by such transforms, usually resulting in at best a scaled invariance, such as the Gaussian function. Further work is required to mathematically prove this result and in determining the analytical properties of the fractal and categorizing their different types.

C. Finite Iterative Reconstruction

We simulated an MR imaging example by taking measurements via k-space trajectories and showed the performance of the proposed method when compared to the conventional radial reconstruction of figure 2 and a sparse CS MR reconstruction method [36] with 30 dB SNR. Figure 8 shows the simulated performance of these methods and the proposed ChaoS method of MR imaging of the Shepp-Logan phantom image. Additional figures for different reduction factors and the Cameraman image are provided as supplementary material.

We have assumed a Gaussian noise model as errors in MR complex signals usually conform to a Gaussian distribution in both real and imaginary components with only the magnitude images being of a Rician or Rayleigh distribution, depending on SNR [57]. We evaluated the quality of each method through metrics such as root mean squared error (RMSE), peak signal-to-noise ratio (PSNR), structural similarity (SSIM) [58] and visual information fidelity (VIF) [59] with the same level of sampling. The latter two are known as perceptual metrics that have been shown to outperform most other metrics (including PSNR) on public subjective viewing image databases [60]. The random sampling was selected as suggested by Majumdar [44, Fig. 2.8(b)] to ensure full 2D incoherence and best fidelity.

Figure 2 shows the k-space sampling utilized for this simulation and the Ghosts present on the initial (uncorrected) reconstruction from the limited imaging data. The CS method utilized the same number of sample points as the finite iterative methods but with additional introduced tiling near the DC coefficient of a radius of 16 coefficients. Table I shows the various metrics used to evaluate the proposed ChaoS scheme

TABLE I
PHANTOM RECONSTRUCTION PERFORMANCE

	Metric	Radial	Compressed Sens. [36]	ChaoS
Simulated	RMSE	16.85	2.18	**1.15**
	PSNR	23.59	41.37	**46.93**
	SSIM	0.39	0.94	**0.99**
	VIF	0.56	0.91	**0.91**
MR Experiment	RMSE	2.03	0.79	**0.22**
	PSNR	41.98	50.14	**61.18**
	SSIM	0.43	0.79	**0.87**
	VIF	0.55	0.83	**0.98**

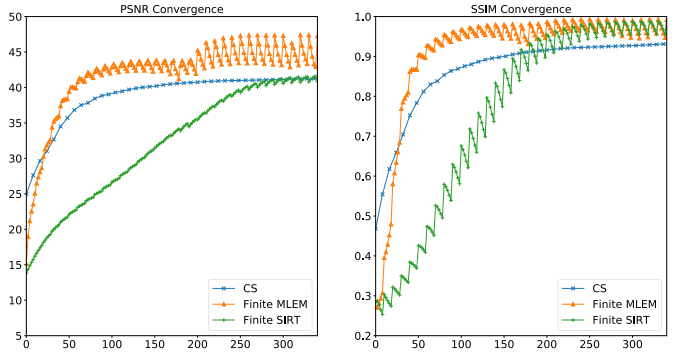

Fig. 9. The convergence performance of the proposed ChaoS fMLEM and fSIRT methods for simulated MR measurements. The oscillations are caused by the non-local means denoising applied at regular intervals (10 iterations in this case) to perturb the current estimate out of local minima. Since the image is consistent within the periodic projections, the system continues to converge to the maximum likelihood solution while the denoising algorithm steadily dampens the Ghosts out of existence.

compared to the radial and CS methods for the Shepp-Logan phantom.

We found that non-local means smoothing [61] applied periodically worked well for dampening the Ghost artifacts. Figure 9 shows the (SSIM and PSNR) convergence characteristics of the proposed method for the Shepp-Logan phantom in the MR imaging simulation, while figure 10 shows the convergence properties given different values of redundancy K, and hence different projection sampling rates, for fixed image size and number of iterations.

The simulation was implemented in-house using the Python programming language via Numpy and Scipy libraries [62] with additional algorithms (such as image denoising) utilized from Scikit-Image [63]. The pyFFTW implementation of the FFT algorithm was also found to be faster than the FFTPACK implementation in Scipy probably because of the mature and prime-sized FFT algorithms available in FFTW [64]. All simulations were computed on an Intel i7-2600K 3.4 GHz with 16GB of RAM on Windows 10. The algorithms used in this work have been made open source [48].

Figure 10 also shows that the reconstruction convergence degrades as the redundancy parameter K is reduced. This is to be expected as there is more ambiguity and less SNR in the measurements corresponding to the reduction in the imaging data. The degradation could also be due to the dependence of the convergence on not only the number of projections, which

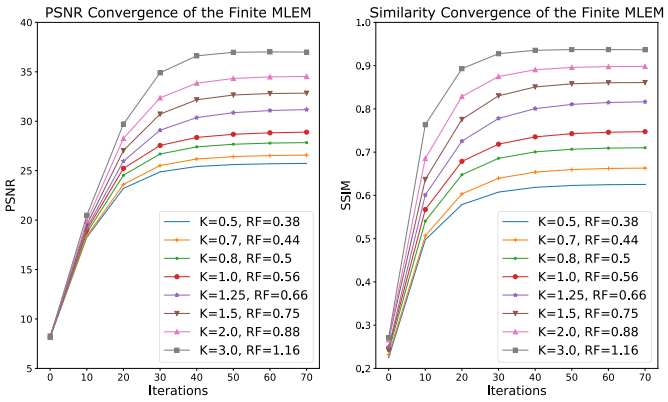

Fig. 10. The convergence performance of the proposed fMLEM method for MR imaging simulation with varying redundancies or projection sampling rates K. Since K affects the number of projections, and therefore the reduction factor, the subset size s would also need tuning to improve convergence.

is dictated by K, but also on the number of subsets s per K, since the selection of s was fixed for this simulation.

D. MR Experiment

Finally, we conducted an MR experiment of a phantom in the laboratory to demonstrate the proposed ChaoS scheme on acquired MR imaging data. A single slice of a phantom was scanned using a Bruker BioSpec 94/30 small animal 9.4T MR scanner (Ettlingen, Germany) with an image size of $p = 257$ using the FLASH (Cartesian) sequence. The phantom was that of a series of Lego blocks in a plastic tube filled with a liquid solution made up of 2.62 g (0.0448 mol) NaCl and 2.14 g (0.0047 mol) $NiSO_4 \cdot 6H_2O$ per 1000 g distilled water. The Bruker mouse head volume coil (diameter of 40mm) with quadrature drive was used to acquire images.

The Cartesian space was then sampled according to patterns shown in figures 2 and 8. This corresponded to the sampling of pixel locations of the fractal pattern for $p = 257$, $s = 16$, 250 iterations and $K = 1.2$ corresponding to a reduction factor of 2 (i.e. 50% of the full Cartesian sampling). The same reduction factor and sampling rate was used to sample pixel locations of the Cartesian space for the radial and CS methods as a comparison. Since full random sampling in MR imaging is not feasible, the standard CS sampling approach was conducted with randomness along phase encoding (columns) as described by Lustig *et al.* [36]. The non-local means smoothing algorithm was utilized for the regularization of the ChaoS method. The result of the complex-valued reconstruction is shown in figure 11. The reconstruction took 174 seconds using a serial implementation of the complex-valued fMLEM algorithm using Numpy and pyFFTW. The RMSE, PSNR, SSIM and VIF of the radial, CS and proposed ChaoS methods are shown in table I when utilizing half of the fully sampled Cartesian reconstructed image. The reduction factor was also varied and the reconstructions computed for each of the methods. The resulting PSNRs of the results are shown in figure 12 when compared to a full Cartesian reconstruction.

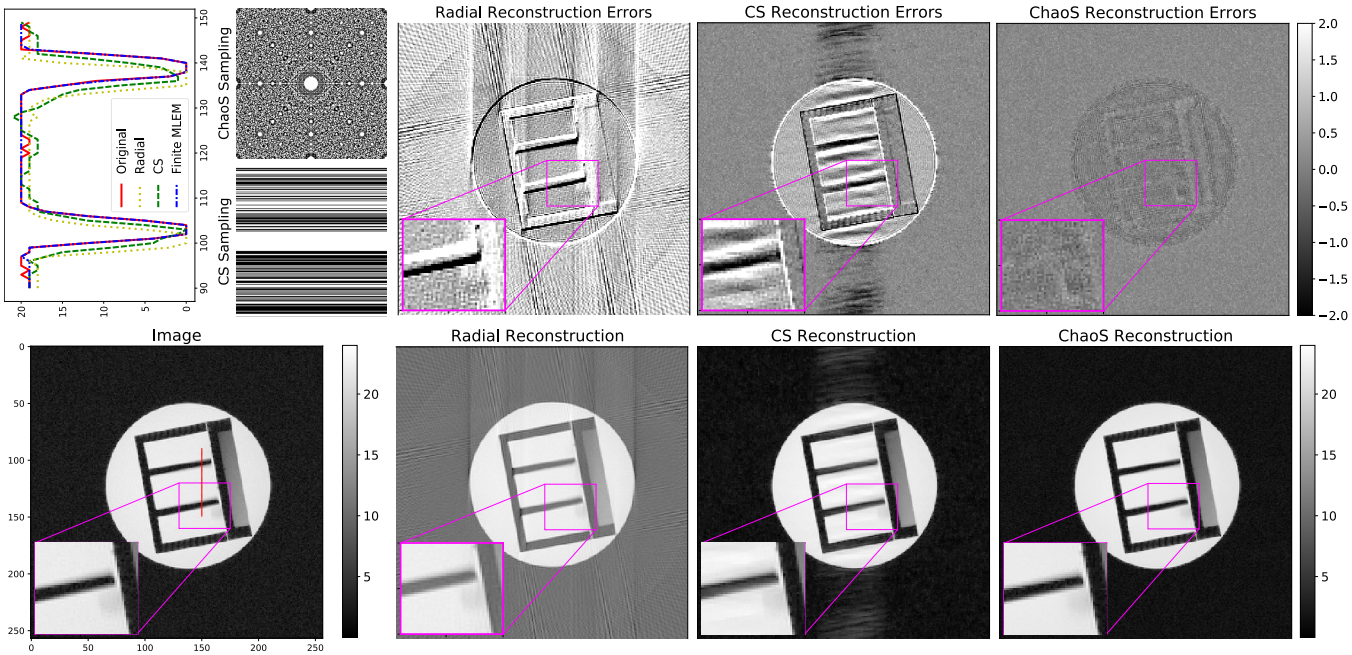

Fig. 11. The full FLASH (Cartesian), radial, CS and proposed ChaoS (bottom row, left to right) reconstructions of a Lego phantom acquired using a Bruker BioSpec small animal 9.4T scanner with $N = 256$ and $p = 257$. The radial, CS and proposed ChaoS algorithms have the same sampling rate corresponding to a reduction factor of 2 (i.e. half of the full DFT sampling) with the latter utilizing the parameters $s = 16$, $K = 1.2$, 128 periodic lines and 250 iterations. The radial reconstruction utilized the sampling given in figure 2. The images were gamma corrected for visualization with $\gamma = 0.5$.

The initial MR experiment with a Lego phantom scanned at 9.4T shown in figure 11 shows promise and behaves as predicted by the MR simulation experiments. The only complication found required using a complex-valued fMLEM algorithm extended from the one proposed by Choi *et al.* [65] that adjusts the EM algorithm to allow arbitrary ranges of image values in the reconstruction to remove the non-negativity constraint of the fMLEM. This is important in complex-valued images as the real and imaginary parts can be both positively and negatively valued. The upper and lower bounds used for this ABfMLEM algorithm were in the order of magnitude of the expected bit depth of the image. However, this algorithm effectively requires an additional projection and back-projection step per iteration rather than one, hence requiring an additional two FFTs.

IV. Discussion

The proposed ChaoS method was found to be robust in the presence of noise and to arbitrary complex-valued measurements as can be seen from figures 8 and 11. Both the simulated and experimental results showed promising performance over the radial and CS methods. Despite having the optimal sampling pattern for fidelity through 2D incoherence [44] and a non-linear optimiser (a non-linear conjugate gradient (CG) in this case) in the simulation, the reconstruction from the CS method had visible artifacts when compared to the proposed ChaoS scheme.

In both the simulations and the MR imaging experiment that involve significant under-sampling (50%-12.5% of full sampling), the turbulent Ghosts are eventually removed with the combination of search for the maximum likelihood solution and dampening the Ghosts with image denoising. The image independent nature of the Ghosts allows edge preserving and texture reducing smoothing to dampen the Ghosts over time. This forced the optimisation out of local minima and approach the global solution. This can be seen in the oscillatory nature of the convergence in figure 9.

In MR imaging, the random sampling pattern for the CS method is usually one that only has 1D coherence, because MR measurements are optimized for linear acquisition and not 2D non-linear trajectories. As a result, the MR experiment showed that the CS method had significant 1D artifacts due to only having 1D coherence, meaning the Ghost artifacts in this dimension could not be adequately removed. The fractal sampling on the other hand, had no such limitation as it remains unchanged from the patterns used in the simulation. This shows that the proposed ChaoS method has greater potential in real-world applications to MR imaging and other areas where linear sampling is preferred.

The non-local means denoising algorithm [61] was found to be the best performing regularization in MR experiments contrast to CS, where total variation algorithms are preferred. This is probably due to the turbulent nature of the Ghosts, since the turbulence manifests as texture features more than pseudo-random noise, and the non-local means algorithm is more suited to artifacts with texture. Therefore, other (non-linear) regularization algorithms, such as the bilateral filter [66], may also prove successful.

Although both fMLEM and fSIRT are designed with different noise models in mind, namely Poisson and Gaussian respectively, the effects of noise is very small compared to the effect of the Ghosts and therefore application of either method is justified. The reconstruction errors are unstructured

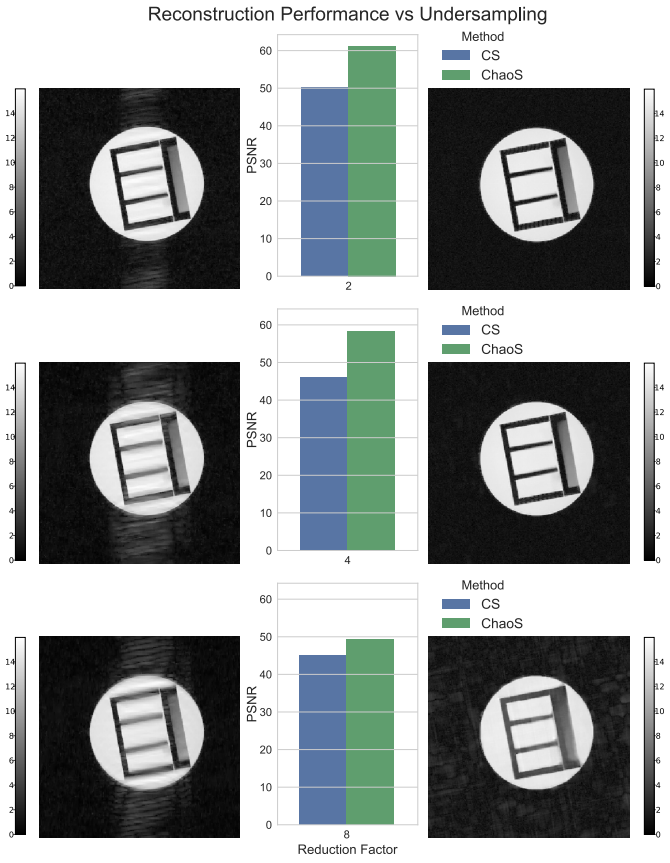

Fig. 12. The reconstruction performance of the proposed ChaoS method compared to CS for a Lego phantom acquired using a Bruker BioSpec small animal 9.4T scanner. The reduction factors 2, 4, and 8 correspond to 50%, 25% and 12.5% of the fully sampled FLASH (Cartesian) sequence data.

as expected and there are no apparent issues with convergence (see figure 9).

Transform sparsity could also be introduced into the proposed method, although shown to be not necessary, to compute more convex optimisation type solutions. Do and Vetterli [67] have already shown how the slices of the DFT can naturally map to a wavelet representation. Randomizing imaging data via the DRT has also been explored and may be useful in this endeavor [68]. Figure 8 also shows that MR acquisitions should be possible and could prove a more natural fit for sparse MR image reconstruction than CS because the geometry of k-space is equivalent to DFT space allowing the use of discrete lines in acquisition. These lines could be implemented via a series of radial lines.

There are a couple of limitations of the proposed method however. Firstly, we have assumed that the measurements are acquired with a fractal pattern. In reality, the patterns are only approximately fractals (or pseudo-fractals), since image sizes are usually small (i.e. $N \ll 2^{16}$) and errors are present in sampling positions in real world applications, such as diagnostic imaging. Thus, one obtains more ideal turbulence at higher image resolutions and therefore the proposed method would likely work better at very large image sizes. The imperfection of the fractal at lower resolutions can be seen in figure 8 utilized for the MR simulation. The result is that the Ghosts are not perfectly turbulent, retaining some minimal structure. We have shown however, that $p = 257$ is sufficient for MR measurements and the proposed method yielded favorable results in these contexts (see figures 8 and 11). In the same way pseudo-random numbers are still suitable for use as random numbers, we believe that pseudo-fractals will have similar utility.

A second limitation is that the finite iterative reconstruction algorithms developed in this work requires the use of non-linear smoothing algorithms, such as non-local means, which usually have high computational complexity, although it is not required for every iteration. Faster algorithms of these types of methods tend to be approximations of the desired smoothing outcomes. However, when $K > 2$ and p was the closest prime number greater than kN for $k > 1$, it was found that the fMLEM algorithm did not require any smoothing to remove the Ghosts directly providing the desired result. In these cases, ChaoS is not dependent on any assumptions of image appearance as it relies on the EM algorithm and the DRT, where the latter can recover an arbitrary finite image with compact support and the maximum likelihood solution suffices directly because the Katz criterion is satisfied allowing theoretically exact reconstruction.

There are a number of other interesting questions that arise regarding the finite fractal presented in this work. The fractal is very reminiscent of a diffraction pattern in crystallography. It would be interesting to see if such a fractal could be physically realized based on previous work on "Diffractals" [69] and fractal gratings [70]. More generally, it remains to be seen if the fractal can provide further insight into number theory, as the distances of Farey sequence from the origin is equivalent to the Riemann hypothesis, which relates to the distribution of prime numbers [71].

More crucially, it remains to be seen whether other fractals can be utilized for making limited measurements, particularly in DFT space. For example, the Julia set shown in figure 3 naturally exists in the complex plane. Given recent work on studying the actual pattern of DFT coefficients utilized in medical image reconstruction [41] showed that there is a certain distribution of coefficients mostly near the origin, fractal patterns that sample near the origin, such as the Dragon or Julia sets, could prove very useful in medical image reconstruction.

V. Conclusion

This work proposed the Chaotic Sensing (ChaoS) methodology that utilizes fractal sampling for the recovery of images from significantly under-sampled imaging data. ChaoS produces turbulent mixing of image information resulting in chaotic Ghost artifacts, yet in a deterministic fashion that facilitates finite iterative reconstruction through discrete tomographic projections (see figure 7). The artifacts are removed through a combination of obtaining the maximum likelihood solution and dampening these artifacts via smoothing. The proposed scheme was made possible via a newly discovered fractal in the DFT (see figure 1), whose symmetry makes it invariant in both image and DFT spaces. The work was evaluated and compared to compressed sensing using simulations

on test images and MR phantom experiments (see figures 8 and 11). It was found to be robust to noise, positive and negative complex-valued measurements and artifacts, while offering promising performance over compressed sensing with the same amount of under-sampling. Further work is required in studying the mathematical properties of the new fractal and in applying the proposed methodology to other applications.

ACKNOWLEDGMENTS

The authors from the University of Queensland would like to acknowledge a faculty philanthropic grant.

REFERENCES

[1] T. Nyholm and J. Jonsson, "Counterpoint: Opportunities and challenges of a magnetic resonance imagingâĽ"only radiotherapy work flow," *Seminars Radiat. Oncol.*, vol. 24, no. 3, pp. 175–180, Jul. 2014.

[2] K. T. Smith, D. C. Solmon, and S. L. Wagner, "Practical and mathematical aspects of the problem of reconstructing objects from radiographs," *Bull. Amer. Math. Soc.*, vol. 83, no. 6, pp. 1227–1270, 1977.

[3] A. K. Louis and W. Törnig, "Ghosts in tomography—The null space of the radon transform," *Math. Methods Appl. Sci.*, vol. 3, no. 1, pp. 1–10, 1981.

[4] R. N. Bracewell and J. A. Roberts, "Aerial smoothing in radio astronomy," *Austral. J. Phys.*, vol. 7, pp. 615–640, Dec. 1954.

[5] B. F. Logan, "The uncertainty principle in reconstructing functions from projections," *Duke Math. J.*, vol. 42, no. 4, pp. 661–706, 1975.

[6] M. B. Katz, *Questions of Uniqueness and Resolution in Reconstruction From Projections* (Lecture Notes in Biomathematics). Springer-Verlag, 1977.

[7] A. K. Louis, "Nonuniqueness in inverse radon problems: The frequency distribution of the ghosts," *Math. Zeitschrift*, vol. 185, no. 3, pp. 429–440, Sep. 1984.

[8] B. Mandelbrot, "How long is the coast of britain? Statistical self-similarity and fractional dimension," *Science*, vol. 156, no. 3775, pp. 636–638, May 1967.

[9] B. Mandelbrot, *The Fractal Geometry of Nature*, 1st ed. San Francisco, CA, USA: Freeman, 1982.

[10] E. N. Lorenz, "Deterministic nonperiodic flow," *J. Atmos. Sci.*, vol. 20, no. 2, pp. 130–141, Mar. 1963.

[11] M. J. Feigenbaum, "Quantitative universality for a class of nonlinear transformations," *J. Statist. Phys.*, vol. 19, no. 1, pp. 25–52, 1978.

[12] D. Ruelle and F. Takens, "On the nature of turbulence," *Commun. Math. Phys.*, vol. 20, no. 3, pp. 167–192, 1971.

[13] L. F. Richardson, *Weather Prediction by Numerical Process*. Cambridge, U.K.: Cambridge Univ. Press, 2007.

[14] N. Normand, J. V. Guedon, O. Philippé, and D. Barba, "Controlled redundancy for image coding and high-speed transmission," *Proc. SPIE*, vol. 2727, pp. 1070–1081, Feb. 1996.

[15] G. T. Herman and R. Davidi, "Image reconstruction from a small number of projections," *Inverse Problems*, vol. 24, no. 4, p. 17, 2008.

[16] R. Gordon, R. Bender, and G. T. Herman, "Algebraic reconstruction techniques (ART) for three-dimensional electron microscopy and X-ray photography," *J. Theor. Biol.*, vol. 29, no. 3, pp. 471–481, Dec. 1970.

[17] P. Gilbert, "Iterative methods for the three-dimensional reconstruction of an object from projections," *J. Theor. Biol.*, vol. 36, no. 1, pp. 105–117, Jul. 1972.

[18] A. P. Dempster, N. M. Laird, and D. B. Rubin, "Maximum likelihood from incomplete data via the EM algorithm," *J. Roy. Statist. Soc. B, Methodol.*, vol. 39, no. 1, pp. 1–38, 1977.

[19] L. A. Shepp and Y. Vardi, "Maximum likelihood reconstruction for emission tomography," *IEEE Trans. Med. Imag.*, vol. MI-1, no. 2, pp. 113–122, Jan. 1982.

[20] H. M. Hudson and R. S. Larkin, "Accelerated image reconstruction using ordered subsets of projection data," *IEEE Trans. Med. Imag.*, vol. 13, no. 4, pp. 601–609, Dec. 1994.

[21] P. J. Green, "Bayesian reconstructions from emission tomography data using a modified EM algorithm," *IEEE Trans. Med. Imag.*, vol. 9, no. 1, pp. 84–93, Mar. 1990.

[22] C. Byrne, "Iterative algorithms for deblurring and deconvolution with constraints," *Inverse Problems*, vol. 14, no. 6, p. 1455, 1998.

[23] J. Mehta and A. Majumdar, "RODEO: Robust DE-aliasing autoencoder for real-time medical image reconstruction," *Pattern Recognit.*, vol. 63, pp. 499–510, Mar. 2017.

[24] J. E. Boyd and J. J. Little, "Complementary data fusion for limited-angle tomography," in *Proc. IEEE Comput. Soc. Conf. Comput. Vis. Pattern Recognit.*, Jun. 1994, pp. 288–294.

[25] D. L. Donoho, "For most large underdetermined systems of linear equations the minimal ℓ^1-norm solution is also the sparsest solution," *Commun. Pure Appl. Math.*, vol. 59, no. 6, pp. 797–829, 2006.

[26] J. Wright and Y. Ma, "Dense error correction via ℓ_1-minimization," *IEEE Trans. Inf. Theory*, vol. 56, no. 7, pp. 3540–3560, Jul. 2010.

[27] M. Vetterli, P. Marziliano, and T. Blu, "Sampling signals with finite rate of innovation," *IEEE Trans. Signal Process.*, vol. 50, no. 6, pp. 1417–1428, Jun. 2002.

[28] S. S. Chandra, I. D. Svalbe, J. Guédon, A. M. Kingston, and N. Normand, "Recovering missing slices of the discrete Fourier transform using ghosts," *IEEE Trans. Image Process.*, vol. 21, no. 10, pp. 4431–4441, Oct. 2012.

[29] E. J. Candès, J. Romberg, and T. Tao, "Robust uncertainty principles: Exact signal reconstruction from highly incomplete frequency information," *IEEE Trans. Inf. Theory*, vol. 52, no. 2, pp. 489–509, Feb. 2006.

[30] D. L. Donoho, "Compressed sensing," *IEEE Trans. Inf. Theory*, vol. 52, no. 4, pp. 1289–1306, Apr. 2006.

[31] E. J. Candès and T. Tao, "Near-optimal signal recovery from random projections: Universal encoding strategies?" *IEEE Trans. Inf. Theory*, vol. 52, no. 12, pp. 5406–5425, Dec. 2006.

[32] Y. C. Eldar and G. Kutyniok, Eds., *Compressed Sensing: Theory and Applications*. Cambridge, U.K.: Cambridge Univ. Press, 2012.

[33] I. Daubechies, M. Defrise, and C. De Mol, "An iterative thresholding algorithm for linear inverse problems with a sparsity constraint," *Commun. Pure Appl. Math.*, vol. 57, no. 11, pp. 1413–1457, Nov. 2004.

[34] S. S. Chen, D. L. Donoho, and M. A. Saunders, "Atomic decomposition by basis pursuit," *SIAM J. Sci. Comput.*, vol. 20, no. 1, pp. 33–61, Jan. 1998.

[35] Y. C. Pati, R. Rezaiifar, and P. S. Krishnaprasad, "Orthogonal matching pursuit: Recursive function approximation with applications to wavelet decomposition," in *Proc. Conf. Rec. 27th Asilomar Conf. Signals, Syst. Comput.*, vol. 1, Nov. 1993, pp. 40–44.

[36] M. Lustig, D. Donoho, and J. M. Pauly, "Sparse MRI: The application of compressed sensing for rapid MR imaging," *Magn. Reson. Med.*, vol. 58, no. 6, pp. 1182–1195, Dec. 2007.

[37] J. Huang, S. Zhang, and D. Metaxas, "Efficient MR image reconstruction for compressed MR imaging," *Med. Image Anal.*, vol. 15, no. 5, pp. 670–679, Oct. 2011.

[38] R. Baraniuk and P. Steeghs, "Compressive radar imaging," in *Proc. IEEE Radar Conf.*, Apr. 2007, pp. 128–133.

[39] J. Yang, J. Wright, T. S. Huang, and Y. Ma, "Image super-resolution via sparse representation," *IEEE Trans. Image Process.*, vol. 19, no. 11, pp. 2861–2873, Nov. 2010.

[40] G. H. Glover and D. C. Noll, "Consistent projection reconstruction (CPR) techniques for MRI," *Magn. Reson. Med.*, vol. 29, no. 3, pp. 345–351, Mar. 1993.

[41] F. Knoll, C. Clason, C. Diwoky, and R. Stollberger, "Adapted random sampling patterns for accelerated MRI," *Magn. Reson. Mater. Phys., Biol. Med.*, vol. 24, no. 1, pp. 43–50, Jan. 2011.

[42] J. Cooley, P. Lewis, and P. Welch, "The finite Fourier transform," *IEEE Trans. Audio Electroacoust.*, vol. AU-17, no. 2, pp. 77–85, Jun. 1969.

[43] S. Ma, W. Yin, Y. Zhang, and A. Chakraborty, "An efficient algorithm for compressed MR imaging using total variation and wavelets," in *Proc. IEEE Conf. Comput. Vis. Pattern Recognit. (CVPR)*, Jun. 2008, pp. 1–8.

[44] A. Majumdar, *Compressed Sensing for Magnetic Resonance Image Reconstruction*. Cambridge, U.K.: Cambridge Univ. Press, Feb. 2015.

[45] Z. Baharav, "Fractal arrays based on iterated functions system (IFS)," in *Proc. IEEE Antennas Propag. Soc. Int. Symp.*, vol. 4, Jul. 1999, pp. 2686–2689.

[46] R. Schmidt and A. Webb, "Improvements in RF shimming in high field MRI using high permittivity materials with low order pre-fractal geometries," *IEEE Trans. Med. Imag.*, vol. 35, no. 8, pp. 1837–1844, Aug. 2016.

[47] G. Julia, "Mémoire sur l'itération des fonctions rationnelles," *J. Math. Pures Appl.*, vol. 1, pp. 47–246, 1918.

[48] S. S. Chandra. (2018). Chaotic Sensing. University of Queensland, St Lucia, QLD, Australia. [Online]. Available: https://github.com/shakes76/ChaoS

[49] G. H. Hardy and E. M. Wright, *An Introduction to the Theory of Numbers*, 5th ed. Oxford, U.K.: Clarendon, 1979.

[50] F. Matúš and J. Flusser, "Image representation via a finite radon transform," *IEEE Trans. Pattern Anal. Mach. Intell.*, vol. 15, no. 10, pp. 996–1006, Oct. 1993.
[51] A. M. Grigoryan, "New algorithms for calculating the discrete Fourier transforms," *J. Vichislit. Matem. Mat. Fiziki*, vol. 25, no. 9, pp. 1407–1412, 1986.
[52] I. Svalbe and D. van der Spek, "Reconstruction of tomographic images using analog projections and the digital Radon transform," *Linear Algebra Appl.*, vol. 339, nos. 1–3, pp. 125–145, 2001.
[53] S. S. Chandra, N. Normand, A. Kingston, J. Guedon, and I. Svalbe, "Robust digital image reconstruction via the discrete Fourier slice theorem," *IEEE Signal Process. Lett.*, vol. 21, no. 6, pp. 682–686, Jun. 2014.
[54] S. Chandra and I. Svalbe, "Exact image representation via a number-theoretic radon transform," *IET Comput. Vis.*, vol. 8, no. 4, pp. 338–346, Aug. 2014.
[55] R. A. Redner and H. F. Walker, "Mixture densities, maximum likelihood and the EM algorithm," *SIAM Rev.*, vol. 26, no. 2, pp. 195–239, 1984.
[56] D. S. Lalush and M. N. Wernick, "Chapter 21—Iterative image reconstruction," in *Emission Tomography*. San Diego, CA, USA: Academic, 2004, pp. 443–472.
[57] H. Gudbjartsson and S. Patz, "The Rician distribution of noisy MRI data," *Mag. Reson. Med.*, vol. 34, no. 6, pp. 910–914, 1995.
[58] Z. Wang, A. C. Bovik, H. R. Sheikh, and E. P. Simoncelli, "Image quality assessment: From error visibility to structural similarity," *IEEE Trans. Image Process.*, vol. 13, no. 4, pp. 600–612, Apr. 2004.
[59] H. R. Sheikh and A. C. Bovik, "Image information and visual quality," *IEEE Trans. Image Process.*, vol. 15, no. 2, pp. 430–444, Feb. 2006.
[60] W. Lin and C.-C. Jay Kuo, "Perceptual visual quality metrics: A survey," *J. Vis. Commun. Image Represent.*, vol. 22, no. 4, pp. 297–312, May 2011.
[61] J. Darbon, A. Cunha, T. F. Chan, S. Osher, and G. J. Jensen, "Fast nonlocal filtering applied to electron cryomicroscopy," in *Proc. 5th IEEE Int. Symp. Biomed. Imag.*, May 2008, pp. 1331–1334.
[62] S. van der Walt, S. C. Colbert, and G. Varoquaux, "The NumPy array: A structure for efficient numerical computation," *Comput. Sci. Eng.*, vol. 13, no. 2, pp. 22–30, 2011.
[63] S. van der Walt *et al.*, "Scikit-image: Image processing in Python," *PeerJ*, vol. 2, p. e453, Jun. 2014.
[64] M. Frigo and S. G. Johnson, "The design and implementation of FFTW3," *Proc. IEEE*, vol. 93, no. 2, pp. 216–231, Feb. 2005.
[65] J. Choi, D. Kim, C. Oh, Y. Han, and H. Park, "An iterative reconstruction method of complex images using expectation maximization for radial parallel MRI," *Phys. Med. Biol.*, vol. 58, no. 9, p. 2969, 2013.
[66] C. Tomasi and R. Manduchi, "Bilateral filtering for gray and color images," in *Proc. Int. Conf. Comput. Vis.*, Washington, DC, USA, Jan. 1998, pp. 839–846.
[67] M. N. Do and M. Vetterli, "The finite ridgelet transform for image representation," *IEEE Trans. Image Process.*, vol. 12, no. 1, pp. 16–28, Jan. 2003.
[68] G.-W. Ou, D. P.-K. Lun, and B. W.-K. Ling, "Compressive sensing of images based on discrete periodic radon transform," *Electron. Lett.*, vol. 50, no. 8, pp. 591–593, Apr. 2014.
[69] M. V. Berry, "Diffractals," *J. Phys. A, Math. General*, vol. 12, no. 6, p. 781, 1979.
[70] J. Wang, W. Zhang, Y. Cui, and S. Teng, "Fresnel diffraction of fractal grating and self-imaging effect," *Appl. Opt.*, vol. 53, no. 10, pp. 2105–2111, Apr. 2014.
[71] J. Franel, "Les suites de farey et le probléme des nombres premiers," *Gottinger Nachr*, pp. 191–201, 1924.

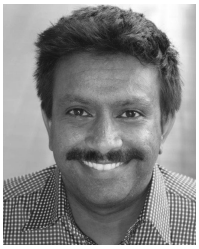

Shekhar S. Chandra was born in Suva, Fiji, in 1980. He received the B.Sc. degree in computer science from The University of the South Pacific, Fiji, and the B.Sc. degree (Hons.) in physics and astrophysics and the Ph.D. degree in theoretical physics from Monash University, Australia, in 2001, 2006, and 2010, respectively. He is currently a Lecturer of biomedical engineering with the School of Information Technology and Electrical Engineering, The University of Queensland, Australia.

He completed a Post-Doctoral Fellowship in medical image analysis from the Australian e-Health Research Centre, CSIRO. His current research interests include improving magnetic resonance reconstruction, image/signal processing, machine learning, and medical image analysis.

Gary Ruben was born in Melbourne, Australia, in 1967. He received the B.E., M.Eng.Sc., Grad.Dip.Sc., B.Sc.(Hons), and Ph.D. degrees from Monash University in 1989, 1999, 2005, 2006, and 2010, respectively. He is currently a Researcher with the School of Physics and Astronomy, Monash University. His research interests include X-ray scatter, emission tomography, and singular optics.

Jin Jin was born in China in 1980. He received the B.Eng. degree in biomedical engineering from Shanghai Jiaotong University, Shanghai, China, in 2003, and the master's and Ph.D. degrees in biomedical engineering from The University of Queensland, Brisbane, Australia, in 2009 and 2013, respectively. He is currently a Senior Scientist with Siemens Heathineers, USA. He is also an Adjunct Fellow with The University of Queensland. His research interests include the development of radiofrequency systems, imaging sequences, and reconstruction methods involving magnetic resonance imaging.

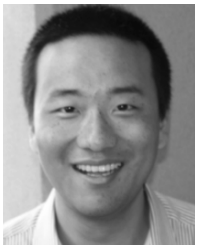

Mingyan Li was born in Dongying, Shandong, China, in 1985. He received the B.Eng. degree (Hons.) from the Qingdao University of Science and Technology, Qingdao, China, in 2007, and the M.Eng. and Ph.D. degrees in biomedical engineering from The University of Queensland (UQ), Australia, in 2010 and 2015, respectively.

He is currently a Post-Doctoral Fellow of biomedical engineering with the School of Information Technology and Electrical Engineering, UQ. His current research interests include development of novel RF technology for ultra-high-field magnetic resonance imaging (MRI), MRI image reconstruction and acceleration, multiple imaging modalities integration, such as MRI-LINAC, non-Cartesian MRI reconstruction, gradient nonlinearity and distortion correction, MR–electrical property tomography, and metamaterial application on MRI.

Andrew M. Kingston was born in Brisbane, Australia, in 1978. He received the B.Sc. degree, the B.Eng. degree (Hons.), and the Ph.D. degree in physics from Monash University in 1999, 2002, and 2006, respectively.

He held a post-doctoral position with the IRCCyN Laboratory, Ecole Polytechnique de l'Universite de Nantes. He is currently a Research Fellow with the Department of Applied Mathematics, Research School of Physics and Engineering, The Australian National University. His research interests are centered around computed tomography and the associated Radon transform (both continuous and discrete forms).

Imants D. Svalbe was born in Ballarat, Australia, in 1952. He received the B.Sc. degree (Hons) in physics and the Ph.D. degree in nuclear physics from The University of Melbourne, Australia, in 1974 and 1979, respectively.

He was an Invited Visiting Professor with the University of Nantes. He is currently a Senior Lecturer with the School of Physics, Monash University, Clayton Campus, Australia, where he teaches physics and medical imaging to radiography students. His principal research interests are focused on discrete effects in digital image processing. He was an Associate Editor of the *Pattern Recognition Letters*.

Stuart Crozier received the Ph.D. and D.Eng. degrees in biomedical engineering. He was an Inaugural Professor of biomedical engineering with The University of Queensland. He is currently an Associate Dean (Research) with the Faculty of Engineering Architecture and IT, The University of Queensland. He has authored over 220 journal papers and holds 30 patents in the field of medical imaging. He has supervised over 35 Ph.D. students to graduation in the field. His main contributions have been to the development of applications and engineering innovation in magnetic resonance imaging (MRI). Several of his innovations have been adopted by industry with the majority of MRI systems worldwide containing technology he co-invented. He was a recipient of the Clunies Ross Medal for research with a societal benefit in 2012. He is an ATSE Fellow and a fellow of The Institute of Physics, U.K. He is a Deputy Editor of the *Magnetic Resonance in Medicine*.